EFFECT OF FRICTION ON THE ZEL'DOVICH–VON NEUMANN–DÖRING TO CHAPMAN–JOUGUET TRANSITION

by

SUSHMA RAO

Presented to the Faculty of the Graduate School of
The University of Texas at Arlington in Partial Fulfillment
of the Requirements
for the Degree of

MASTER OF SCIENCE IN AEROSPACE ENGINEERING

THE UNIVERSITY OF TEXAS AT ARLINGTON

August 2010

To Pratik, my mother and my sister

ACKNOWLEDGEMENTS

At the culmination of my Master's thesis, I would like to thank everyone who inspired and guided me throughout my research.

Firstly, I would like to thank my advisor Dr Frank Lu for believing in me and giving me the opportunity to do original research. I am extremely grateful for his constant guidance. I would also like to thank Dr Donald Wilson for his guidance and support.

Though speaking about my mother's contribution in my thesis would be a very small acknowledgement to her influence on me, I believe that the choices she made and the life that she led set a very high standard for me to try and reach. She was a constant motivation and emotional support during all my graduate life. To say the least I owe her my utmost respect .

I would also like to acknowledge here, the wall who stood next to me throughout my struggles was my now husband Pratik Donde. He not only stood by but was also was a very integral part of my eternal struggles during the years of graduate life and particularly my thesis research. His constant nudge kept me going and no words can describe my gratitude. My mentor and my worst critique lead me through the various ups and downs of my thesis and graduate studies.

I would also like to thank my sister for always encouraging me in my endeavors. She was quintessential elder sister who pushed me to reach higher and last longer.

I would also like to thank Eric M. Braun for his help for the Cantera coding and also Ronnachai Vutthivithayarak for his cheerfull help and support.

May 28, 2010

ABSTRACT

EFFECT OF FRICTION ON THE ZEL'DOVICH–VON NEUMANN–DÖRING TO CHAPMAN–JOUGUET TRANSITION

Sushma Rao, MS

The University of Texas at Arlington, 2010

Supervising Professor: Dr. Frank Lu

Detonation theory proposes Chapman-Jouguet state of equilibrium due to the sonic speed of the products relative to the wave. Experimental observations however indicated the existence of a sub-Chapman-Jouguet state. The dissertaion proposes that friction plays a role in defining such a sub-optimal state in detonation wave propagation in ducts. The problem is addressed analytically by decoupling the friction losses from the chemical reactions. The non-equilibrium conditions associated with detonation is modeled by detailed chemistry.

TABLE OF CONTENTS

LIST OF FIGURES

NOMENCLATURE

a	Speed of sound
f	Fanning friction factor
g	Acceleration due to gravity
h	Enthalpy
$\dot{m}$	Mass flux per unit area
q	Difference in enthalpy of formation of reactants and products
x	Reaction zone length
z	Vertical distance from the ground
C_p	Specific heat at constant pressure
C_v	Specific heat at constant volume
D	Cross-sectional diameter
M	Mach No
P	Static pressure
P_t	Total pressure
R	Gas constant
T	Static temperature
T_t	Total temperature
γ	Specific heat ratio
δW	Work done by the fluid
δQ	Heat transfer to the tube walls
ρ	Density
Δs	Change in entropy between reactants and products

Subscript

CJ	Chapman–Jouguet
ZND	Zel'dovich–von Neumann–Döring
0	Reactant states
1	Product states

CHAPTER 1

INTRODUCTION

The motivation for studying detonations dates back to the 18th century and was initiated by Stokes [1, 2]. Current research in this area is motivated by its wide application in areas such as propulsion, industrial safety, accident investigation and explosive and manufacturing. The chemical reaction zone in which rapid reactions occur, is termed the combustion wave. Combustion wave characteristics are essential in understanding detonation physics. In this section, the characteristics of combustion waves are discussed.

1.1 Combustion waves

Figure 1.1 depicts a combustion wave traveling through a reactive gaseous mixture in a tube in a reference frame fixed on the wave. Ignition at the right end of the tube causes the combustion wave to propagate towards the left with a constant velocity u_0, further igniting the reactants in its path. In the figure, the subscripts 0 and 1 denote the state of the unburned gases ahead of the wave and the the state of the burned gases behind the wave respectively. The duct is assumed to be very long and with a constant area.

There are two kinds of combustion waves, namely deflagration and detonation. The speed at which the combustion wave propagates classifies it into these two categories [3]. When the combustion wave travels at a speed lower than the speed of sound with respect to the downstream gases, it is termed as a deflagration wave. A combustion wave traveling at supersonic speed with respect to the downstream gases

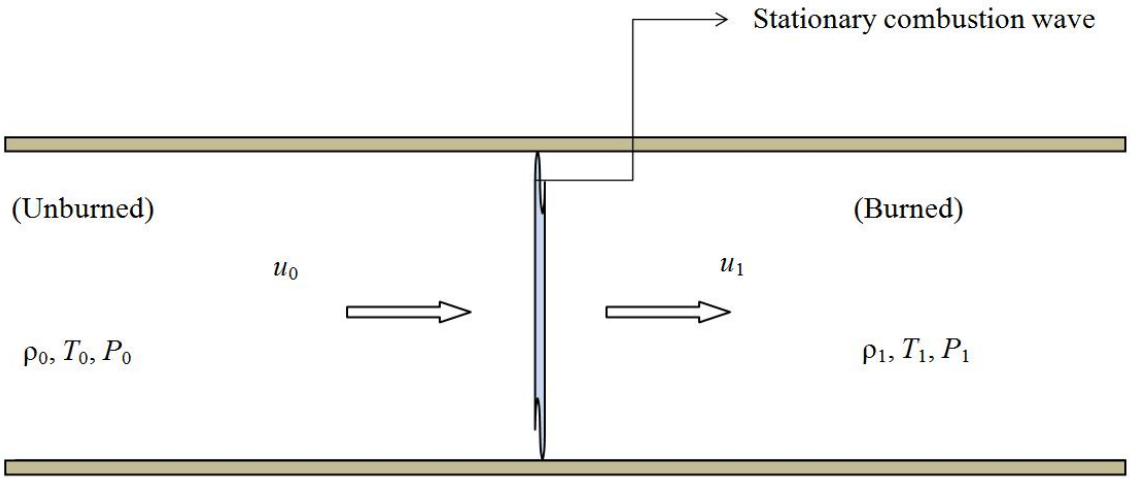

Figure 1.1. Combustion wave in a moving frame of reference.

is called a detonation wave. The leading part of the detonation wave is a strong shock wave. This shock heats the fluid by compressing it, thus triggering chemical reactions, and a balance is attained such that the chemical reaction supports the shock. Hence detonation differs from shock wave only in being diabatic due to the thermal energy released by the chemical reaction [4, 5]. The historical background leading to our current understanding of detonation physics is addressed in the following section.

1.2 Background

Detonations received attention from various scientific communities. Stokes derived the jump conditions across a shock wave using mass and momentum conservation equations in 1848. However, Stokes failed to account for energy conservation [1, 2] leading to an incorrect formulation. Rankine, in 1870, derived the correct jump condition using energy conservation, clearly stating that a shock wave is adiabatic. Hugoniot conducted an identical analysis independently in 1887. Chapman in 1899 postulated that the gases behind the detonation wave travel at the local speed of

sound (in the frame of reference of the moving shock wave) [6]. Jouguet (1905) independently proposed that the detonation velocities should be sonic locally, and additionally showed that the entropy is minimum at the equilibrium point (leading to the Chapman–Jouguet or CJ theory) [7]. Further Zel'dovich, von Neumann and Döring independently derived the one-dimensional steady model (also called the ZND model) of detonation structure in 1940, 1942 and 1943 respectively [8, 9, 10, 11, 12] which considered the finite chemistry after the shock [13, 14]. The next section describes the theories of detonation in greater detail.

1.3 Detonation theories

The Rankine–Hugoniot relations provide a locus of all possible states in an adiabatic system for a given state of the gas, represented by distinct Hugoniot curves. In the current context, we consider two Hugoniot curves: the inert Hugoniot representing the unburnt gases, and a Hugoniot with heat addition representing burnt gases. The process of detonation, however, is diabatic. Detonation theories describe the transition from the inert Hugoniot to the heat addition Hugoniot. In this work, we restrict our discussion to the CJ and ZND theories of detonation.

1.3.1 Chapman–Jouguet (CJ) theory

As shown in figure 1.2, in the Chapman–Jouguet detonation model, gases are compressed by the shock front, simultaneously causing reactions to occur in the shock discontinuity zone. This model assumes that chemical equilibrium is attained immediately after the shock, where the gaseous products are at the sonic speed in the frame of reference of the detonation wave. This is equivalent to the tangency of the Rayleigh line and the heat addition Hugoniot.

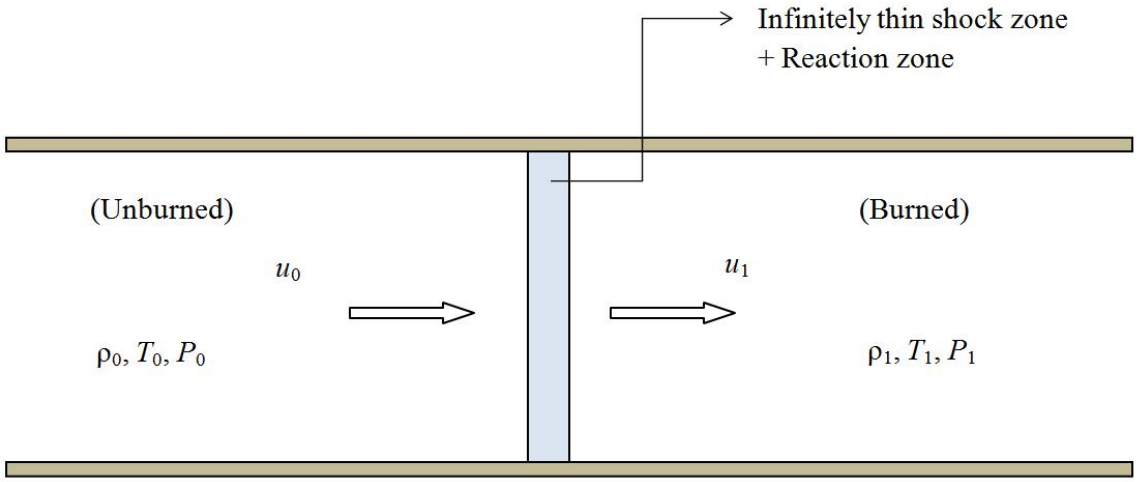

Figure 1.2. Detonation schematic: Chapman–Jouguet theory.

1.3.2 Zel'dovich–von Neumann–Döring (ZND) theory

The ZND theory proposes a different approach for reaching the equilibrium CJ point by incorporating a finite chemical reaction zone behind the shock wave. As shown in figure 1.3, in the ZND model, the detonation wave compresses unburnt gases in the shock front leading to high temperatures and pressures (called the von Neumann spike or the ZND point) [15]. This is followed by finite rate chemical reactions that occur behind the shock front in the reaction zone. Chemical equilibrium is attained after the reaction zone at the CJ point.

The ZND theory provides a more accurate model for detonation by including non-equilibrium chemical kinetics occurring in the reaction zone. The current work aims to examine the transition from the ZND point to the CJ point in the presence of friction. The significance of this research and the methodologies employed will be explained in the next section.

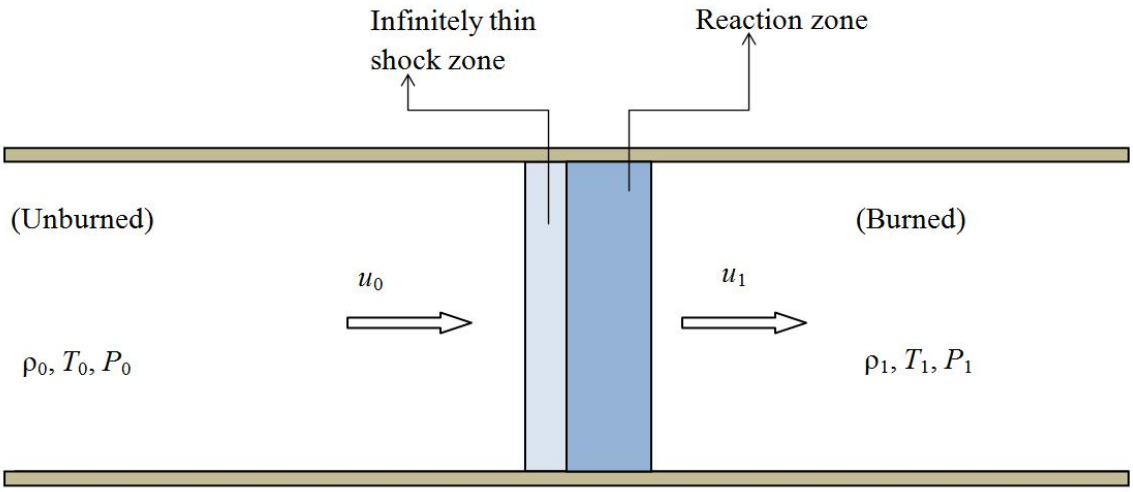

Figure 1.3. Detonation schematic: ZND theory.

1.4 Significance of the research

The propagation of detonation waves in ducts is an important problem in gasdynamics, particularly so with ongoing interest in pulse detonation engines [16, 17, 18]. Analytical and computational approaches to solving detonation wave propagation have generally assumed the problem to be inviscid. Solutions involving the Navier–Stokes equations are expensive and not well developed at the moment. Experimentally, there has been evidence that the fully-developed CJ detonation wave slows down. While there may be various possible mechanisms for the wave to decelerate, a serious possibility is the friction in the duct. This is analogous to the attenuation of shocks in ducts [19] and the effect of boundary layer growth behind a detonation wave [20]. The present work examines one aspect of the attenuation of the detonation wave by considering the friction within the heat release zone between the ZND and the CJ points. The non-equilibrium chemistry within the combustion zone is studied for a stoichiometric hydrogen/oxygen mixture initially at STP. The calculation makes use of Cantera [21]. We assume that at each time (or location within the combustion

front), local thermodynamic equilibrium allows us to identify a thermodynamic state. In other words, the non-equilibrium process from the ZND to the CJ point is replaced by a sequence of states in local thermodynamic equilibrium.

1.5 Thesis outline

In this chapter, the Chapman–Jouguet and Zel'dovich–von Neumann–Döring models were discussed. The background study leading to the current understanding of the two models were introduced. The significance of the ZND to CJ transition was discussed.

In chapter 2, we discuss the governing equations needed to obtain the CJ and ZND points. In chapter 3 we build the analytical solution required to map the transition between CJ and ZND points. We also analyze the effects of friction in the transition model. Finally, in chapter 4 we discuss the results obtained due to the inclusion of friction in the transition model.

CHAPTER 2

GOVERNING EQUATIONS AND METHODOLOGIES

In this chapter we derive the Rankine–Hugoniot relations which relate the conditions across the shock wave. This is followed by the derivation of the Chapman–Jouguet (CJ) and Zel'dovich–von Neumann–Döring (ZND) models of detonation. The initial conditions have been assumed to be 1 atm and 300 K.

2.1 Rankine–Hugoniot relations

We begin with the conservation of mass, momentum and energy across a combustion wave, in the frame of reference of the wave, given by

$$\rho_0 u_0 = \rho_1 u_1 \tag{2.1a}$$

$$P_0 + \rho_0 u_0^2 = P_1 + \rho_1 u_1^2 \tag{2.1b}$$

$$h_0 + q + \frac{u_0^2}{2} = h_1 + \frac{u_1^2}{2} \tag{2.1c}$$

where the subscripts 0 and 1 denote the reactants and the products respectively and q is the amount of heat added per unit mass through combustion, and is equal to the difference between the enthalpies of formation of the reactants and the products. The gases are assumed to be calorically perfect. Hence, using the perfect gas relations, the enthalpy can be expressed as

$$h = \frac{\gamma}{\gamma - 1}\frac{P}{\rho} \tag{2.2}$$

Using (2.1a) and (2.1b), we obtain the relation between pressure and specific volume

$$\frac{P_1 - P_0}{v_0 - v_1} = u_1^2 \rho_1^2 = \dot{m}^2 \tag{2.3}$$

Here $\dot{m}$ is the mass flux and is a constant. Eliminating velocities in the reactants and the products by substituting (2.3) in (2.1c), we obtain the Rankine–Hugoniot equation

$$h_1 - (h_0 + q) = \frac{1}{2}\left(P_1 - P_0\right)\left(v_0 + v_1\right) \tag{2.4}$$

By substituting (2.2) in (2.4) and solving for P_1 we get,

$$P_1 = \frac{h + q - \frac{1}{2}P_0(v_0 + v_1)}{\frac{\gamma}{\gamma - 1}v_1 - \frac{1}{2}(v_0 + v_1)} \tag{2.5}$$

(2.5) can be non-dimensionalized using initial conditions, yielding

$$\frac{P_1}{P_0} = \frac{1 + \gamma - (\gamma - 1)\,\frac{v_1}{v_0} + 2\alpha\,(\gamma - 1)}{1 - \gamma + \frac{v_1}{v_0}\,(\gamma + 1)} \tag{2.6}$$

where

$$\alpha = \frac{q}{P_0 v_0}$$

is the nondimensional heat release. In figure 2.1, Hugoniot curves are constructed using equation (2.6). The inert Hugoniot curve corresponds to $\alpha = 0$, whereas the heat addition Hugoniot curve uses α corresponding to the heat addition due to stoichiometric oxyhydrogen combustion.

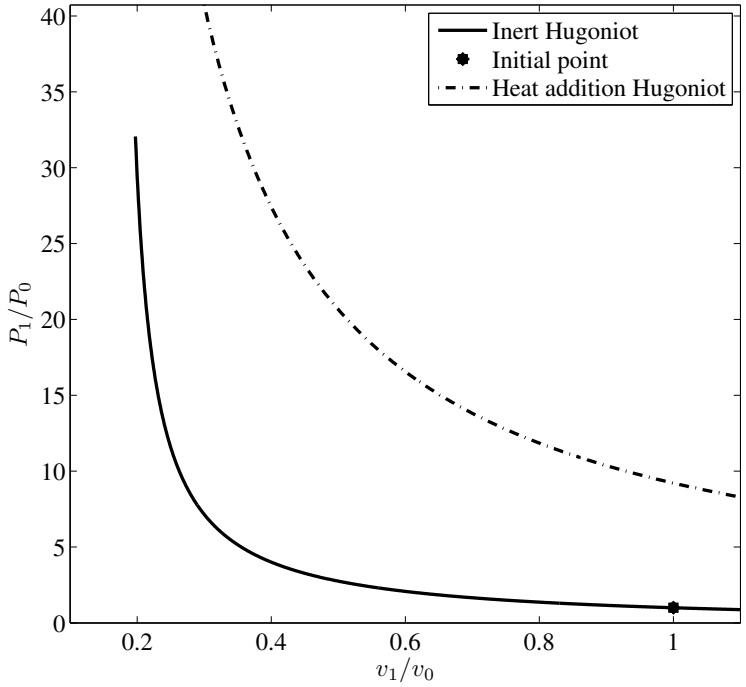

Figure 2.1. P–v diagram showing the inert and heat addition Hugoniots.

For a calorically perfect gas, the integrated Gibbs equation relates the change in entropy with changes in other properties of the gas, as shown in

$$\begin{aligned} \Delta s &= C_v \log \frac{T_1}{T_0} + R \log \frac{v_1}{v_0} \\ &= C_p \log \frac{T_1}{T_0} - R \log \frac{P_1}{P_0} \\ \frac{\Delta s}{R} &= \frac{\gamma}{\gamma - 1} \log \frac{T_1}{T_0} - \log \frac{P_1}{P_0} \end{aligned} \tag{2.7}$$

Using (2.6) and (2.7), the Hugoniot curves can be plotted in a T–s diagram as shown in figure 2.2.

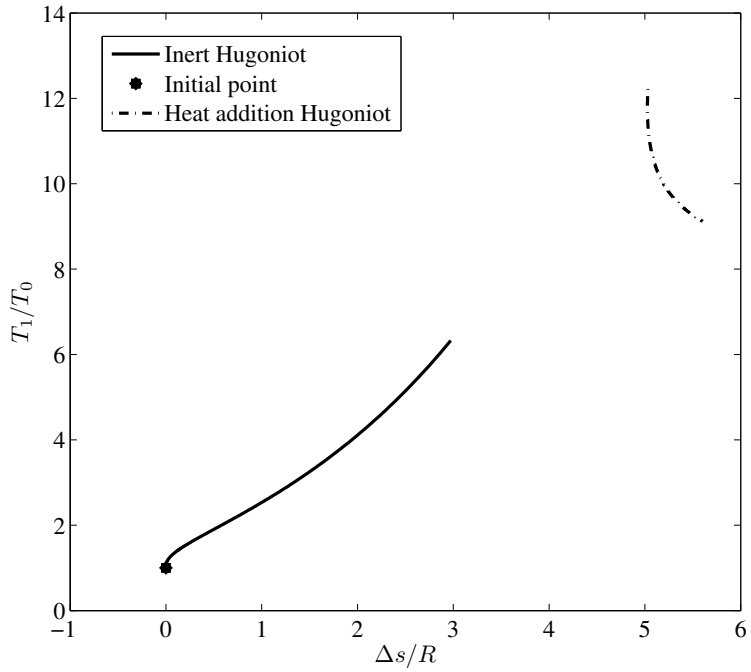

Figure 2.2. T–s diagram showing the inert and heat addition Hugoniots.

2.2 Rayleigh line and the CJ point

The Chapman–Jouguet theory postulates the transition from the initial STP to the CJ point through a Rayleigh line. The CJ point is the point of tangency between the Rayleigh line and the heat addition Hugoniot curve.

For a calorically perfect gas, the speed of sound upstream is defined as $a_0 = \sqrt{\gamma R T_0}$ and Mach number of the combustion wave is given by $M_0 = \frac{u_0}{a_0}$. The continuity and momentum equations given by (2.1a) and (2.1b) can be written in terms of the combustion wave Mach number to yield

$$\frac{P_1}{P_0} = \left(1 + \gamma_0 M_0^2\right) - \gamma_0 M_0^2 \frac{v_1}{v_0} \tag{2.8}$$

This is the equation of the Rayleigh line. In a P–v diagram, (2.8) represents a straight line with slope $-\gamma_0 M_0^2$. The Rayleigh line is a function of the combustion wave Mach number, which in turn is a function of the detonation velocity. For the problem at hand, the detonation velocity is unknown. We therefore use the CJ theory for finding the CJ point.

2.2.1 Chapman–Jouguet point using the CJ theory

The CJ point is obtained by drawing a line tangent to the heat addition Hugoniot from the initial point. A method for obtaining an analytical expression for the CJ point is explained in this section. Equation (2.6) allows us to construct a heat addition Hugoniot. The slope of the tangent to this curve can be obtained by differentiating (2.6) with respect to v, yielding

$$\frac{dP_{CJ}}{dv_{CJ}} = -\frac{P_0}{v_0\left[1-\gamma+(1+\gamma)\frac{v_{CJ}}{v_0}\right]}\times$$
$$(1+\gamma)\left[1+2\alpha(\gamma-1)+\gamma-(\gamma-1)\frac{v_{CJ}}{v_0}\right]+(1-\gamma)\left[1-\gamma+(1+\gamma)\frac{v_{CJ}}{v_0}\right] \tag{2.9}$$

The slope of the Rayleigh line originating from the initial conditions is given by

$$\frac{dP_{CJ}}{dv_{CJ}} = \frac{P_{CJ}-P_0}{v_{CJ}-v_0} \tag{2.10}$$

By equating (2.9) and (2.10), an analytical expression for v_{CJ} is obtained as

$$v_{CJ} = \frac{-\alpha v_0+\gamma v_0+\gamma^2 v_0+\alpha\gamma^2 v_0+\sqrt{\alpha(\gamma^2-1)(2\gamma-\alpha+\alpha\gamma^2)v_0^2}}{\gamma(\gamma+1)} \tag{2.11}$$

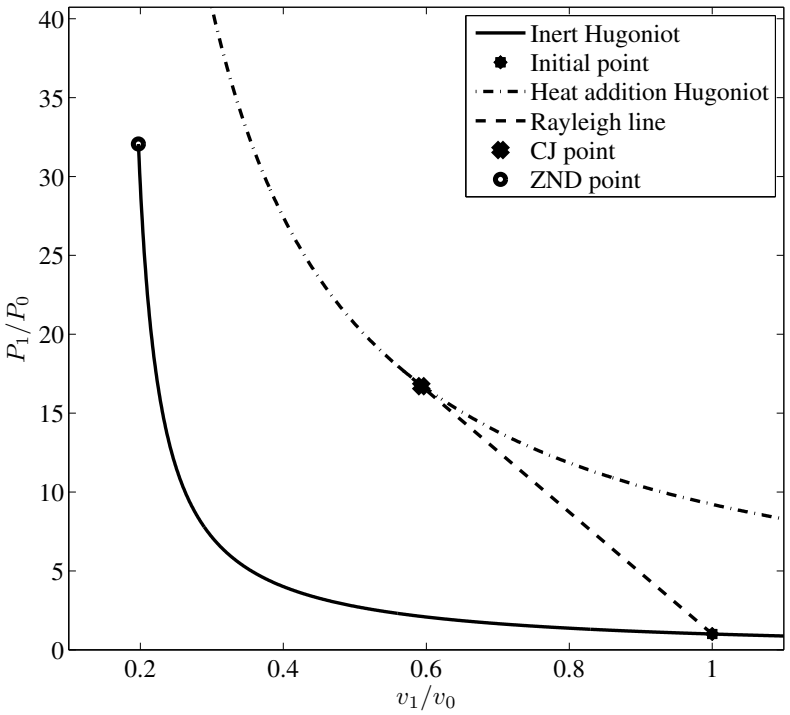

Figure 2.3. $P - v$ diagram showing the Rayleigh process.

The symbolic equation solver Mathematica was used for obtaining (2.11); see Appendix A for details. Once v_{CJ} is known, (2.6) can be used for obtaining P_{CJ}. The Rayleigh line can now be obtained by connecting the CJ point to the initial point.

Figure 2.3 shows the Rayleigh line thus obtained in a P–v diagram. Using (2.8) and (2.7), the Rayleigh process can be plotted in a T–s diagram. Figure 2.4 shows the Rayleigh line representing transition between the inert Hugoniot and the heat addition Hugoniot through the Rayleigh process.

2.2.2 Chapman–Jouguet point using Cantera

Cantera is a collection of open source libraries written in C++ and provides tools for solving problems involving chemical kinetics, thermodynamics and transport

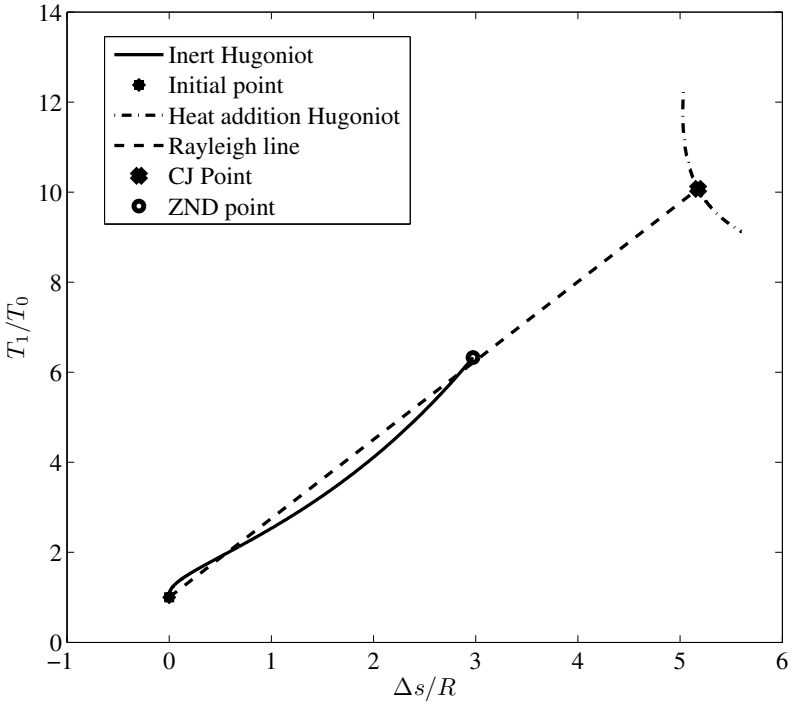

Figure 2.4. T–s diagram showing the Rayleigh process.

processes [22]. In this work, we use Cantera for obtaining solutions to the H_2–O_2 detonation problem. This allows us to take into account non-equilibrium effects by including detailed chemistry and local thermodynamic equilibrium at each time and location.

The properties of the CJ point obtained using the analytical solution developed in this section agree well with those computed using Cantera. Details of these calculations can be found in Appendix C.

2.3 Obtaining the ZND point

The ZND point is the state attained by the gases after shock compression. It is also called the von Neumann spike. We obtain the Mach number of the detona-

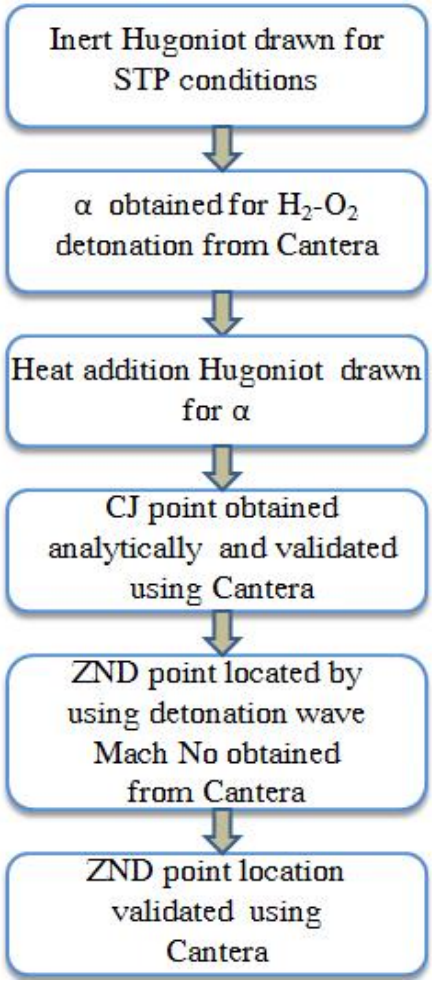

Figure 2.5. Flowchart describing the process of obtaining the CJ and ZND points.

tion wave for H_2–O_2 detonation from Cantera. By using normal shock relations, we analytically obtain properties at the ZND point. The analytical results were verified by Cantera. The P–v diagram in Fig. 2.3 and the T–s diagram in Fig. 2.4 depict the ZND point.

2.4 Summary

In this chapter we derived the Rankine-Hugoniot relations. The heat addition Hugoniot was used for obtaining the CJ point using the CJ detonation theory. The

ZND point was obtained based on the ZND theory of detonation. The methodology to obtain the CJ and ZND points has been summarized in the flowchart 2.5. All results agree well with those obtained from Cantera.

CHAPTER 3

ZND TO CJ TRANSITION

The transition from the ZND point to the CJ point occurs in the reaction zone following the shock compression zone (see figure 1.3). In this chapter we analyze the effect of friction on this transition for H_2–O_2 detonation.

3.1 ZND to CJ transition modeling using Cantera

Cantera includes libraries written in C++ that can be accessed using a Matlab interface. We use Cantera for numerically solving the H_2–O_2 detonation problem with detailed chemistry, assuming local chemical equilibrium. Refer to Appendix C for the Matlab code used for accessing Cantera, written by Eric Braun (graduate student, University of Texas at Arlington).

The path for ZND to CJ transition predicted using Cantera can be approximated well using a straight line in a P–v diagram. The slope of this line is identical to a Rayleigh line originating from the CJ point. Figure 3.1 compares the path for transition modeled using a Rayleigh line with that predicted using Cantera.

3.2 Generalized flow model

In the previous section, we modeled the ZND to CJ transition using Cantera, which accounts for detailed chemistry. In real flows, however, there are many other factors responsible for changes in flow properties, such as wall friction, change in cross-sectional area, heat transfer through the walls, buoyancy effects, etc. [23].

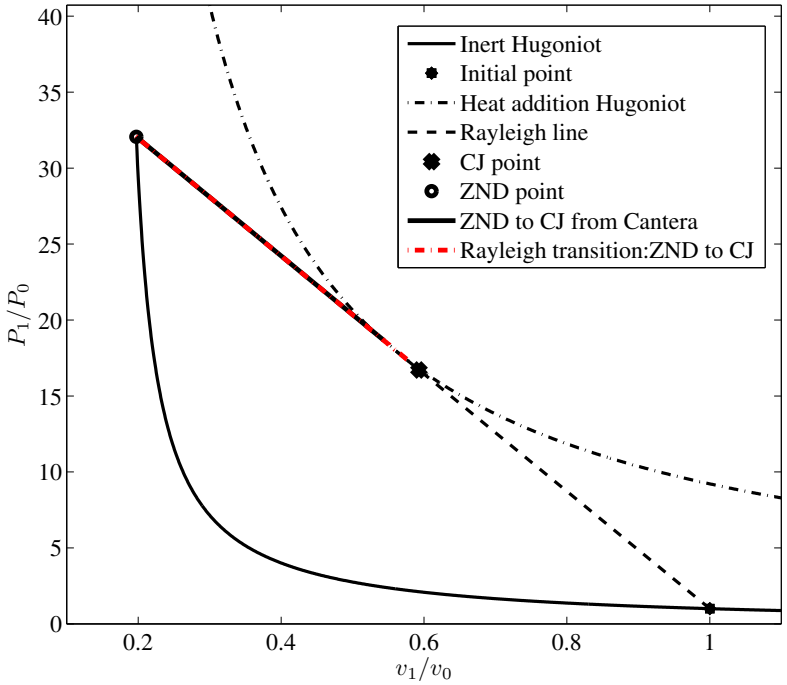

Figure 3.1. P–v diagram showing ZND to CJ transition using Cantera and Rayleigh transition modeling.

By accounting for all of the above in a differential control volume, we come up with the generalized equations for a one-dimensional flow. The continuity, momentum and energy equations for the generalized flow are given by equations (3.1),(3.2) and (3.3) respectively.

$$\frac{d\dot{m}}{\dot{m}} = \frac{d\rho}{\rho} + \frac{dA}{A} + \frac{du}{u} \tag{3.1}$$

$$\begin{aligned} dP + \rho u du + \rho g dz + \frac{\rho u^2}{2}\left(\frac{4f dx}{D}\right) + \frac{\delta D}{A} \\ + \rho u^2 (1-y)\frac{d\dot{m}}{\dot{m}} = 0 \end{aligned} \tag{3.2}$$

Here $4f\,dx/D$ is the effect of wall friction and is termed as the friction factor.

$$\begin{aligned}\delta\dot{W} - \delta\dot{Q} + (\dot{m} + d\dot{m})\left[h + dh + \frac{u^2}{2} + d\left(\frac{u^2}{2}\right) + g(z + dz)\right] \\ -\dot{m}\left(h + \frac{u^2}{2} + gz\right) - d\dot{m}\left(h_i + \frac{u_i^2}{2} + gz_i\right) = 0\end{aligned} \tag{3.3}$$

Neglecting higher order terms, from equation (3.3) we obtain,

$$\begin{aligned}\delta W - \delta Q + dh + d\left(\frac{u^2}{2}\right) + gdz \\ + \left[\left(h + \frac{u^2}{2} + gz\right) - \left(h_i + \frac{u_i^2}{2} + gz_i\right)\right]\frac{d\dot{m}}{\dot{m}} = 0\end{aligned} \tag{3.4}$$

Here the subscript i denotes the properties of the fluid through a secondary inlet (for example, a fuel injector). Also δW and δQ are the work done by the fluid and heat transfer through the walls respectively. Using the definition of total enthalpy, equation (3.4) can be written as

$$\delta W - \delta Q + dH + dH_i = 0 \tag{3.5}$$

where the total enthalpy $H = h + u^2/2 + gz$, and $dH_i = (H - H_i)d\dot{m}/\dot{m}$.

3.2.1 Generalized flow model: perfect gas

For a perfect gas, the generalized flow model can be written in terms of eight distinct flow properties as given in (3.6) [24].

$$\begin{bmatrix} 0 & 1 & 0 & 1 & 0 & 0 & 0 & 0 \\ 1 & 0 & \frac{\gamma M^2}{2} & 0 & \gamma M^2 & 0 & 0 & 0 \\ 1 & -1 & -1 & 0 & 0 & 0 & 0 & 0 \\ 0 & 0 & \frac{1}{2} & -1 & 1 & 0 & 0 & 0 \\ 0 & 0 & 1 & 0 & \frac{(\gamma-1)M^2}{\psi} & 0 & 0 & 0 \\ 1 & 0 & 0 & 0 & \frac{\gamma M^2}{\psi} & -1 & 0 & 0 \\ -1 & 0 & 0 & 0 & -\frac{2\gamma M^2}{1+\gamma M^2} & 0 & 1 & 0 \\ \frac{\gamma-1}{\gamma} & 0 & -1 & 0 & 0 & 0 & 0 & 1 \end{bmatrix} \cdot \begin{bmatrix} \frac{dP}{P} \\ \frac{d\rho}{\rho} \\ \frac{dT}{T} \\ \frac{du}{u} \\ \frac{dM}{M} \\ \frac{dP_t}{P_t} \\ \frac{dF}{F} \\ \frac{ds}{C_p} \end{bmatrix} = \begin{bmatrix} \frac{d\dot{m}}{\dot{m}} - \frac{dA}{A} \\ K + L \\ 0 \\ 0 \\ \frac{dT_t}{T_t} \\ 0 \\ \frac{dA}{A} \\ 0 \end{bmatrix} \tag{3.6}$$

where

$$\begin{aligned} \psi &= 1 + \frac{\gamma - 1}{2} M^2 \\ K &= -\frac{\gamma M^2}{2} \left(\frac{4 f dx}{D} \right) \\ L &= -\gamma M^2 (1 - y) \frac{d\dot{m}}{\dot{m}} \end{aligned}$$

Here the impulse function is defined as $F = PA + \dot{m}u$. In this work, we use the generalized equations for a perfect gas to include the effects of only heat addition and friction.

3.3 Combined flow model: heat addition and friction

A combined flow model is proposed that would represent a flow with wall friction and heat addition. By neglecting other effects, the system (3.6) can hence be written as

$$\begin{bmatrix} 0 & 1 & 0 & 1 & 0 & 0 & 0 & 0 \\ 1 & 0 & \frac{\gamma M^2}{2} & 0 & \gamma M^2 & 0 & 0 & 0 \\ 1 & -1 & -1 & 0 & 0 & 0 & 0 & 0 \\ 0 & 0 & \frac{1}{2} & -1 & 1 & 0 & 0 & 0 \\ 0 & 0 & 1 & 0 & \frac{(\gamma-1)M^2}{\psi} & 0 & 0 & 0 \\ 1 & 0 & 0 & 0 & \frac{\gamma M^2}{\psi} & -1 & 0 & 0 \\ -1 & 0 & 0 & 0 & -\frac{2\gamma M^2}{1+\gamma M^2} & 0 & 1 & 0 \\ \frac{\gamma-1}{\gamma} & 0 & -1 & 0 & 0 & 0 & 0 & 1 \end{bmatrix} \begin{bmatrix} \frac{dP}{P} \\ \frac{d\rho}{\rho} \\ \frac{dT}{T} \\ \frac{du}{u} \\ \frac{dM}{M} \\ \frac{dP_t}{P_t} \\ \frac{dF}{F} \\ \frac{ds}{C_p} \end{bmatrix} = \begin{bmatrix} 0 \\ -\frac{\gamma M^2}{2}\left(\frac{4f dx}{D}\right) \\ 0 \\ 0 \\ \frac{dT_t}{T_t} \\ 0 \\ 0 \\ 0 \end{bmatrix} \tag{3.7}$$

(3.7) is of the form $\mathbf{Ax} = \mathbf{B}$, where matrix $\mathbf{A}$ is the matrix of coefficients and $\mathbf{x}$ is a vector of property changes; $\mathbf{x}$ can be obtained by inverting $\mathbf{A}$ using Cramer's rule. An explicit equation for dM/M can hence be obtained:

$$\frac{dM}{M} = \left(\frac{4f dx}{D}\right)\left(\frac{\gamma M^2 \psi}{2(1-M^2)}\right) + \frac{dT_t}{T_t}\frac{(1+\gamma M^2)\psi}{2(1-M^2)} \tag{3.8}$$

Dividing by dx yields

$$\frac{dM}{dx} = M\left[\frac{4f}{D}\frac{\gamma M^2 \psi}{2(1-M^2)} + \frac{dT_t}{dx}\frac{(1+\gamma M^2)\psi}{2T_t(1-M^2)}\right] \tag{3.9}$$

(3.9) is a non-linear equation, and must be integrated numerically from M_{ZND} to M_{CJ}. Here, M_{ZND} is obtained from the analysis discussed in chapter 2, and $M_{CJ} \equiv 1$. This assumption is consistent with the CJ theory of detonation. The changes in the seven remaining flow properties can be obtained by using the solution of (3.9) and

standard flow relations. We obtain the properties of pressure, specific volume, total temperature and entropy by using the following equations:

$$\frac{P_{CJ}}{P_{ZND}} = \frac{\dot{m}_{CJ}}{\dot{m}_{ZND}} \frac{M_{ZND}}{M_{CJ}} \left[\frac{T_{t_{CJ}} \left(1 + \frac{\gamma - 1}{2} M_{ZND}^2\right)}{T_{t_{ZND}} \left(1 + \frac{\gamma - 1}{2} M_{CJ}^2\right)} \right] \tag{3.10a}$$

$$\frac{\rho_{CJ}}{\rho_{ZND}} = \frac{P_{CJ}}{P_{ZND}} \frac{T_{ZND}}{T_{CJ}} \tag{3.10b}$$

$$\frac{T_{CJ}}{T_{ZND}} = \frac{T_{t_{CJ}} \left(1 + \frac{\gamma - 1}{2} M_{ZND}^2\right)}{T_{t_{ZND}} \left(1 + \frac{\gamma - 1}{2} M_{CJ}^2\right)} \tag{3.10c}$$

The change in entropy can be computed using the integrated Gibbs equation (2.7). See the Matlab code in Appendix B for details.

3.4 Results and discussion

In the previous section a combined flow model was proposed, which takes into account the effects of wall friction. The model provides us with a system of differential equations for changes in the flow properties. In this section we analyze the results obtained from the combined flow model for the transition from ZND to CJ point.

Numerically integrating (3.9), we obtain the Mach number variation in the reaction zone as a function of distance from the leading shock. Using (3.10a), (3.10b), (3.10c), (2.7) and the Mach number variation from the ZND to CJ points, we can plot the changes in the P–v and T–s diagrams. Figures 3.2 and 3.3 show the variation in properties using the combined flow model with different friction factors denoted by $4fdx/D$. Here the Fanning friction factor f is varied from 1×10^{-6} to 1×10^{-2}.

From figure 3.2, we see that the CJ point predicted using the combined flow model occurs at a lower pressure when compared with the CJ point predicted using inviscid analysis. Both, pressure and specific volume at the CJ point reduce as friction

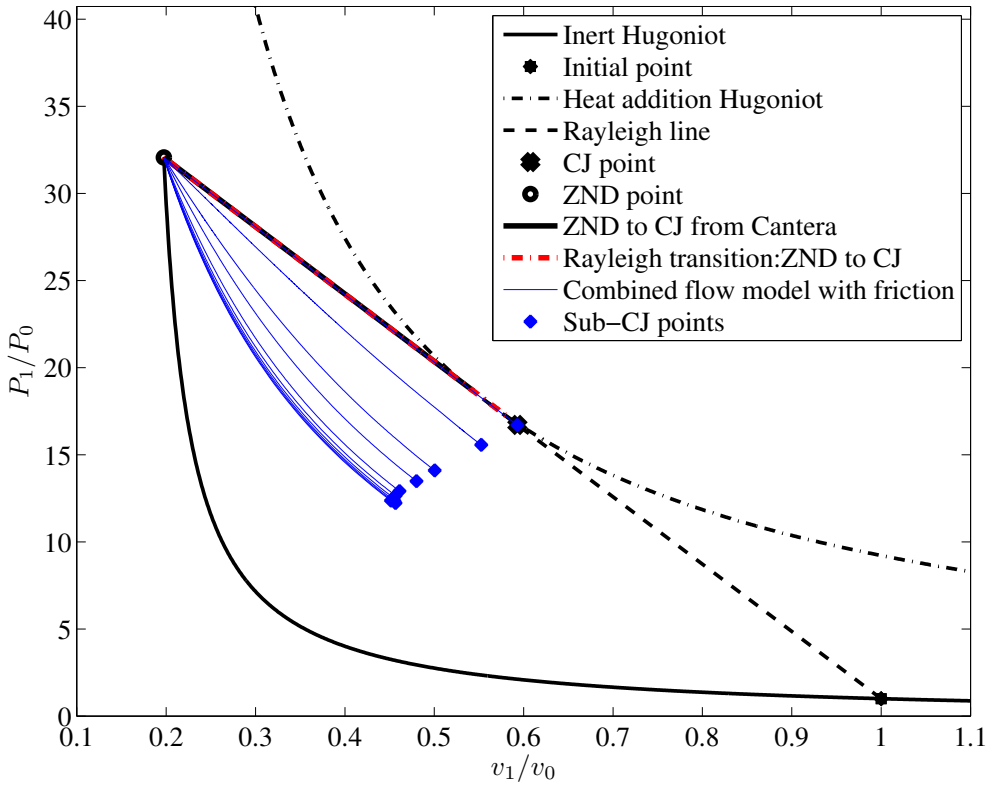

Figure 3.2. P–v diagram showing the transition between ZND to CJ point with combined flow model including heat addition and friction.

at the walls increases. In the T–s diagram shown in figure 3.3, we observe that increasing friction reduces the temperature at the CJ point. Figures 3.4 and 3.5 show the locus of all the CJ points for various friction factors. We observe that with increase in friction factor the CJ point reduces. We also observe that the reduction in the CJ points have a limiting value as the Fanning friction factor reaches 1×10^{-2}.

We obtain a family curves by varying the friction factor, each with its unique CJ point. Hence we propose the existence of a family of Hugoniots corresponding to different CJ points. Figures 3.6 and 3.7 show Hugoniots corresponding to two such CJ points. We infer from the above observations that with increasing friction, the

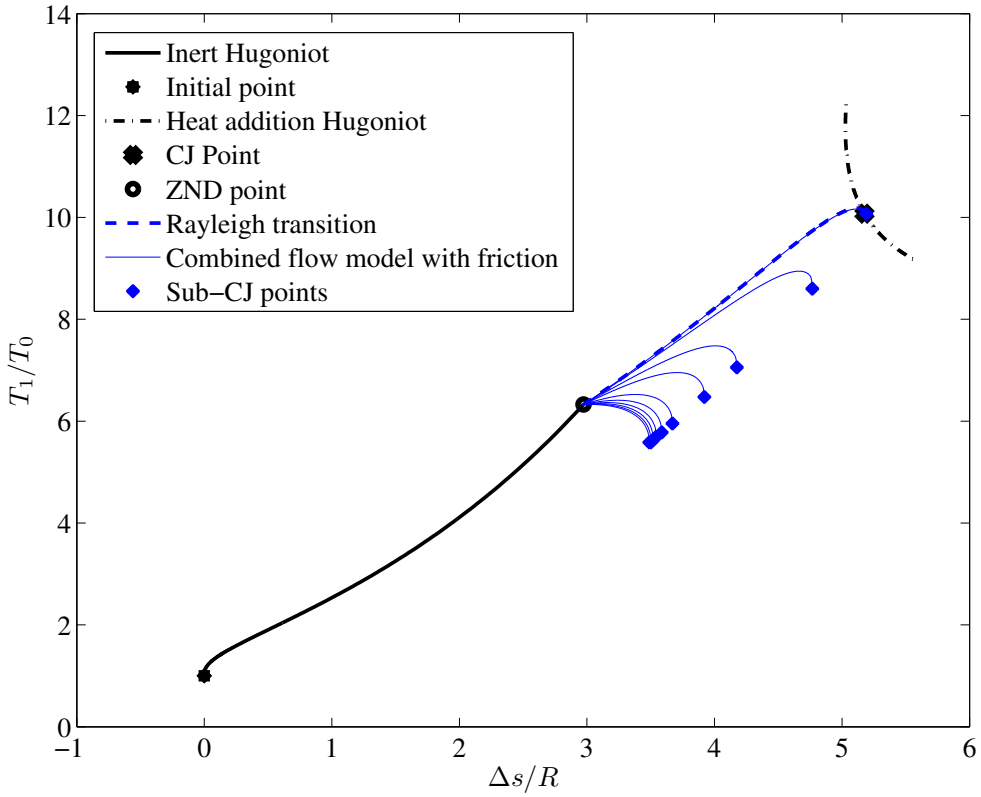

Figure 3.3. $T - s$ diagram showing the transition between ZND to CJ point with combined flow model including heat addition and friction.

non-dimensional heat release α decreases. This implies that the maximum heat added to the heat through combustion reduces.

3.5 Summary

In this chapter, we simplified the generalized one-dimensional flow for a perfect gas to incorporate the effects of only friction, leading to the combined flow model. Flow properties were computed by numerical integration from the ZND point to the CJ point. We analyze the results to observe that the combined flow model gives

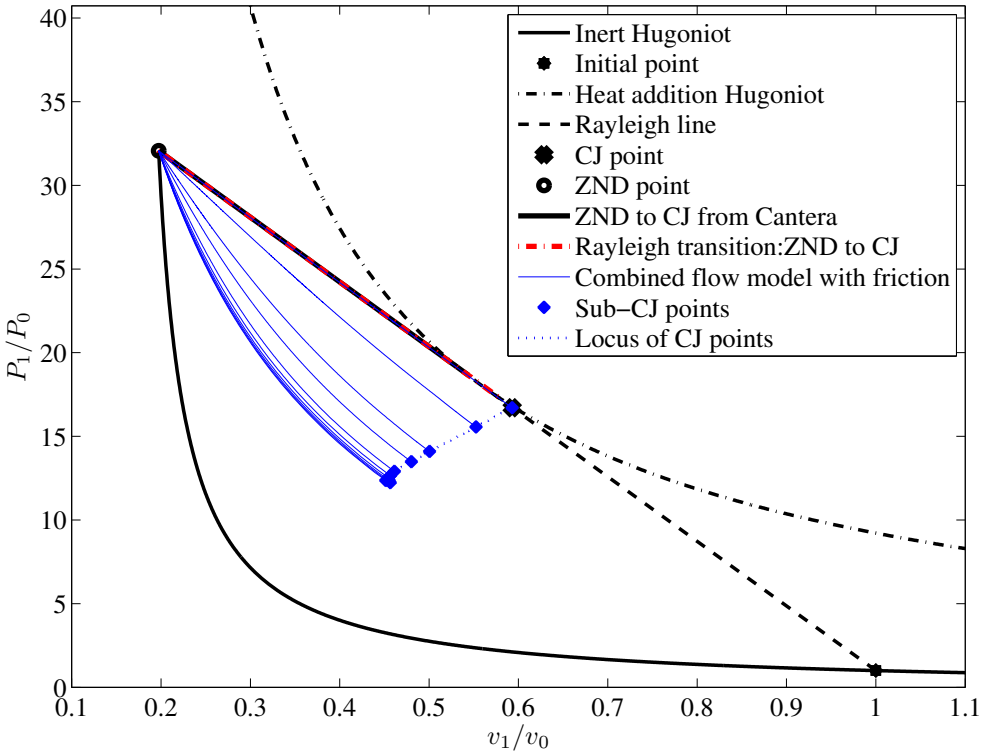

Figure 3.4. P–v diagram showing the transition between ZND to CJ point with combined flow model including heat addition and friction.

us a family of transition curves for different friction factors, which lead to lower CJ points. This concurs with experimental observations. We conclude that a lower CJ point represents a lower α, i.e. heat of reaction. Hence distinct Hugoniot lines pass through these CJ points.

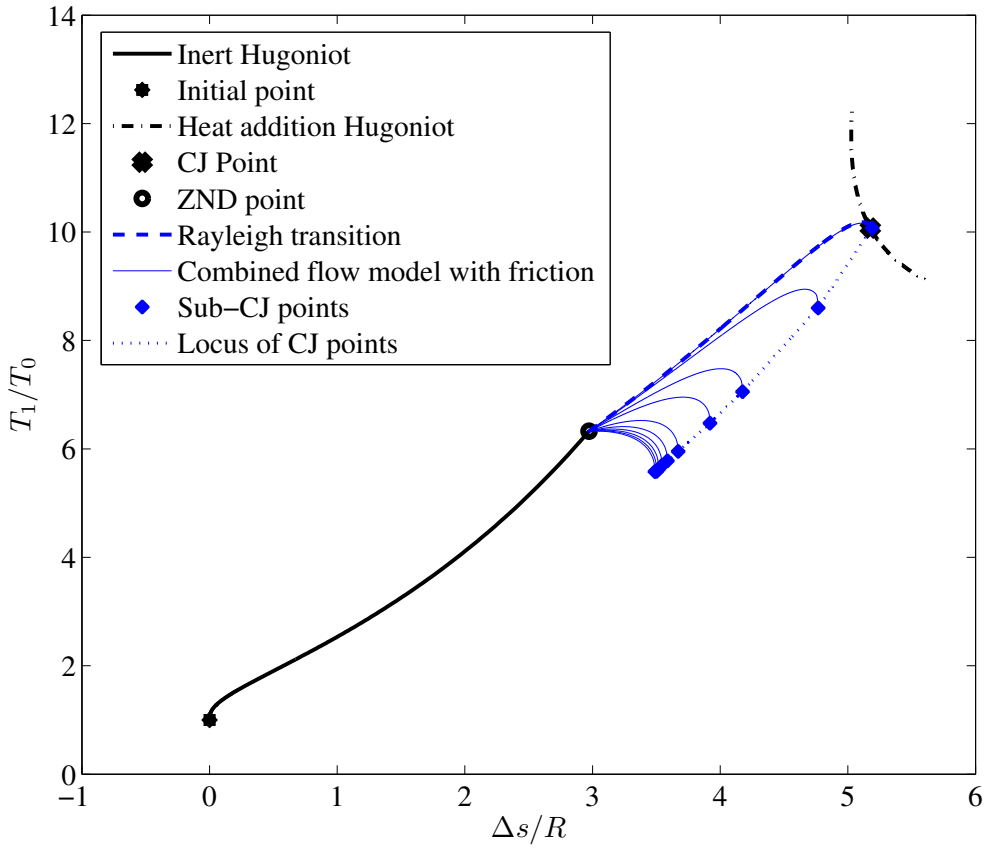

Figure 3.5. $T - s$ diagram showing the transition between ZND to CJ point with combined flow model including heat addition and friction.

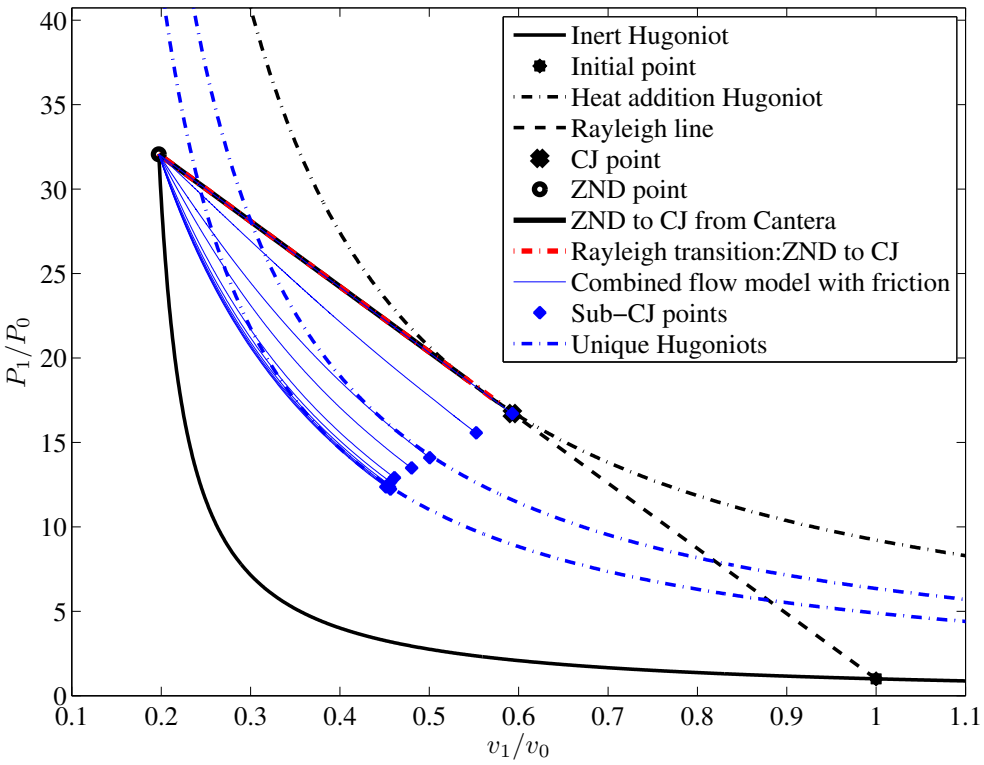

Figure 3.6. P–v diagram showing distinct Hugoniots for arbitrary values of the friction factor.

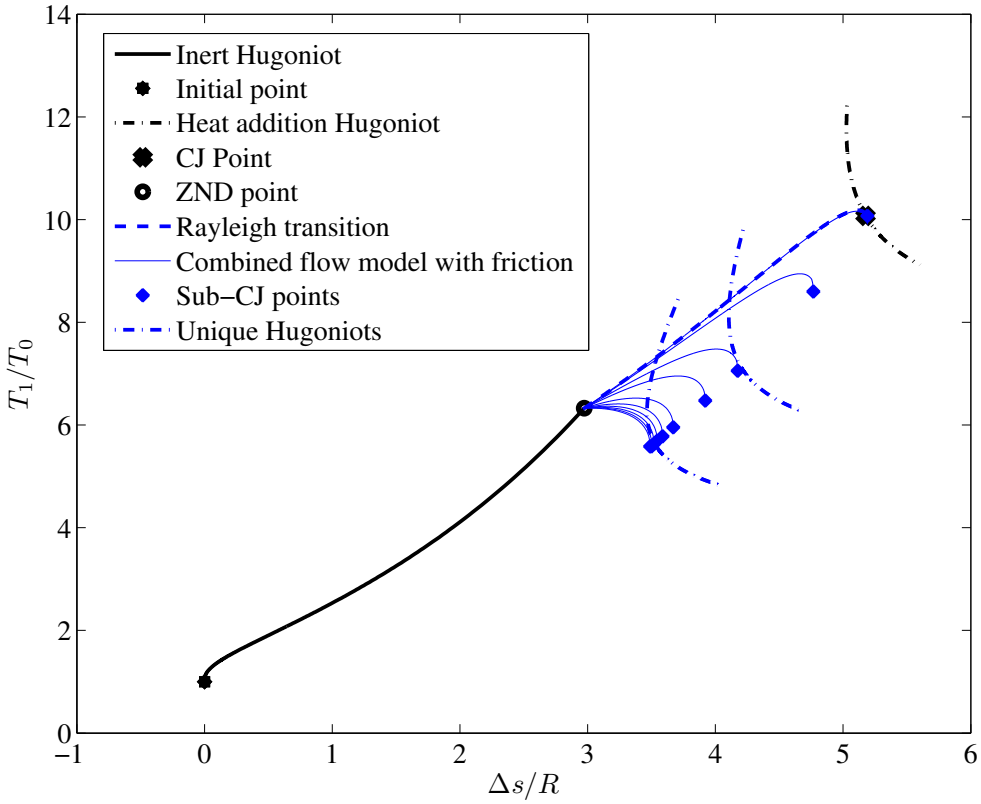

Figure 3.7. T–s diagram showing distinct Hugoniots for arbitrary values of the friction factor.

CHAPTER 4

SUMMARY AND CONCLUSIONS

In chapter 1, we discussed the two established theories of detonation, i.e., the CJ and ZND theories. The CJ theory postulates the existence of a thin reaction zone that travels with the shock. As a result, the transition from the inert Hugoniot to the heat addition Hugoniot can be represented by a Rayleigh line. The Rayleigh line is tangent to the heat addition Hugoniot at the CJ point, which is the point of chemical equilibrium. At the CJ point, the Mach number of the burnt gases is unity in the frame of reference of the detonation wave. This theory, however, fails to account for the non-equilibrium chemistry and an experimentally observed pressure peak, known as the von Neumann spike (also called the ZND point). The ZND theory, on the other hand, postulates the existence of separate shock compression and reaction zones. This allows it to account for the pressure rise at the ZND point. After the ZND point, there are chemical reactions that occur in the reaction zone, and chemical equilibrium is attained at the CJ point. The ZND theory, although a better detonation model, fails to map the transition from the ZND point to the CJ point. In this work, an analytical model has been developed for H_2–O_2 detonation, allowing us to map this transition by including detailed chemistry, and the effect of friction.

In chapter 2, the ZND to CJ transition is obtained numerically using Cantera, which takes the non-equilibrium effects of the reacting gases into account. We showed that this transition can be approximated well by a Rayleigh line.

In chapter 3, a combined flow transition model was constructed incorporating the effects of wall friction (relevant to the shock tube experimental conditions). With

different values of friction factors we obtain a unique curve ending in a unique CJ point. These CJ points agree with the initial premise of a sub-CJ condition found experimentally. We observe from the model that the heat addition Hugoniots passing though these uniques CJ points have a lower heat of reaction α. This leads us to conclude that the family of CJ points have unique Hugoniots passing through them, indicative of their respective heat of reaction α. This implies that an increase in wall friction leads to lower heat addition, since the flow becomes sonic faster. We also observe a reduction in maximum temperature with increase in wall friction.

In conclusion, we see that the analytical model qualitatively agrees with the experimental results, by predicting a sub-CJ state of equilibrium .

4.1 Future work

In the current work, we focus on H_2-O_2 detonation chemistry leading to a model based on the Rayleigh line of heat addition, which is specific to these reactants. An analysis of a larger number of detonation chemistries would allow us to construct a more generalized detonation model. The only input parameters for such a model would be the heat of reaction α and the non-dimensional friction factor $4f\,dx/D$. A detailed analytical model to take into account the effect of friction on the flow behind the detonation wave can be incorporated so as to capture the effects of boundary layer growth, similar to Mirel's problem. A future study could also undertake numerical modeling of the effects of friction.

APPENDIX A

MATHEMATICA: SOLUTION FOR THE CJ POINT

p2 = p1 * (gam + 1 − (gam − 1) * v2/v1 + 2 * (gam − 1) * alpha)/

((gam + 1) * v2/v1 − gam + 1)

$$\frac{\text{p1}\left(1+2\text{alpha}(-1+\text{gam})+\text{gam}-\frac{(-1+\text{gam})\text{v2}}{\text{v1}}\right)}{1-\text{gam}+\frac{(1+\text{gam})\text{v2}}{\text{v1}}}$$

dpdv = p1/v1 * (−(gam − 1) * ((gam + 1) * v2/v1 − (gam − 1))

−((gam + 1) − (gam − 1) * v2/v1 + 2 * alpha * (gam − 1)) * (gam + 1))/

((gam + 1) * v2/v1 − gam + 1)^2

$$\frac{\text{p1}\left(-(1+\text{gam})\left(1+2\text{alpha}(-1+\text{gam})+\text{gam}-\frac{(-1+\text{gam})\text{v2}}{\text{v1}}\right)+(1-\text{gam})\left(1-\text{gam}+\frac{(1+\text{gam})\text{v2}}{\text{v1}}\right)\right)}{\text{v1}\left(1-\text{gam}+\frac{(1+\text{gam})\text{v2}}{\text{v1}}\right)^2}$$

Together[Solve[dpdv==(p2 − p1)/(v2 − v1), v2]]

$$\left\{\text{v2}\to\frac{-\text{alphav1}+\text{gamv1}+\text{gam}^2\text{v1}+\text{alphagam}^2\text{v1}-\sqrt{\text{alpha}(-1+\text{gam}^2)(-\text{alpha}+2\text{gam}+\text{alphagam}^2)\text{v1}^2}}{\text{gam}(1+\text{gam})}\right\},$$

$$\left\{\text{v2}\to\frac{-\text{alphav1}+\text{gamv1}+\text{gam}^2\text{v1}+\text{alphagam}^2\text{v1}+\sqrt{\text{alpha}(-1+\text{gam}^2)(-\text{alpha}+2\text{gam}+\text{alphagam}^2)\text{v1}^2}}{\text{gam}(1+\text{gam})}\right\}$$

APPENDIX B

MATLAB CODE

```
clc;
clear;
%Initial conditions

N=1000;
p1=101325;T1=300; R=573;% Initial condition
v1=R*T1/p1  %Initial v1
v2v1=linspace(1/5.06812290,1.1,N);
gam=1.4014;alpha=0;
Cp=R*gam/(gam-1); s1=Cp;
v1 =

   1.696521095484826

%Shock hugoniot
for i=1:N
p2p1(i)=(gam+1-(gam-1)*v2v1(i)+2*...
(gam-1)*alpha)/((gam+1)*v2v1(i)-gam+1);
% Perfect gas relation
T2T1(i)=p2p1(i)*v2v1(i);
% Integrated Gibbs equation
ds12(i)=Cp*log(T2T1(i))-R*log(p2p1(i));

end
```

Burned gases

```
gam1=1.205666499829051;
R1=692;
%Hugoniot with heat addition
v3v1=linspace(0.3,1.1,N);
H1=4.47e3;U1=0;H2=2.853e6;U2=2.835e3;
Cp1=R1*gam1/(gam1-1);
alpha=((H2+U2^2/2)-(H1+U1^2/2))/(p1*v1)
for i=1:N
    p3p1(i)=(gam1+1-(gam1-1)*v3v1(i)+2*...
(gam1-1)*alpha)/((gam1+1)*v3v1(i)-gam1+1);
    T3T1(i)=p3p1(i)*v3v1(i);%*R/R1;
    ds13(i)=Cp*log(T3T1(i))-R*log(p3p1(i));
end
alpha =

  39.948472949389178
```

Hugo heat

```
%Hugoniot with heat addition
v7v1=linspace(0.23,1.1,N);
U7=1.8e3;
alpha7=((H2+U7^2/2)-(H1+U1^2/2))/(p1*v1)
for i=1:N
    p7p1(i)=(gam1+1-(gam1-1)*v7v1(i)+2*...
(gam1-1)*alpha7)/((gam1+1)*v7v1(i)-gam1+1);
```

```
    T7T1(i)=p7p1(i)*v7v1(i);%*R/R1;
    ds17(i)=Cp*log(T7T1(i))-R*log(p7p1(i));
end
v8v1=linspace(0.2,1.1,N);
U8=0.9e3;
alpha8=((H2+U8^2/2)-(H1+U1^2/2))/(p1*v1)
for i=1:N
    p8p1(i)=(gam1+1-(gam1-1)*v8v1(i)+2*...
(gam1-1)*alpha8)/((gam1+1)*v8v1(i)-gam1+1);
    T8T1(i)=p8p1(i)*v8v1(i);%*R/R1;
    ds18(i)=Cp*log(T8T1(i))-R*log(p8p1(i));
end
alpha7 =

  25.994938917975567


alpha8 =

  18.926876090750437

%Rayleigh line
N=1000;
MZND=5.255;
M2=linspace(0.4114,0.9662364,N);
for i=1:N
```

```
    p4p1(i)=(1+gam*MZND^2)/(1+gam*M2(i)^2);
    v4v1(i)=1/(((1+gam*M2(i)^2)/(1+gam*MZND^2))*(MZND/M2(i))^2);
    T4T1(i)=p4p1(i)*v4v1(i);%*R/R1;
    ds14(i)=Cp*log(T4T1(i))-R*log(p4p1(i));
    prayp1(i)=1+gam*MZND^2-v3v1(i)*MZND*gam;
end
```

ZND point

```
vzndv1=1/5.06812290; pzndp1=32.0637928;
TzndT1=pzndp1*vzndv1;
ds1znd=Cp*log(TzndT1)-R*log(pzndp1);
```

CJ point

```
vcjv1=(gam1-alpha+gam1^2*(1+alpha)-(alpha*(gam1^2-1)*...
(2*gam1-alpha+alpha*gam1^2))^0.5)/(gam1*(gam1+1));
pcjp1=(gam1+1-(gam1-1)*vcjv1+2*...
(gam1-1)*alpha)/((gam1+1)*vcjv1-gam1+1);
TcjT1=pcjp1*vcjv1;%*R/R1;
ds1cj=Cp*log(TcjT1)-R*log(pcjp1);
%Importing Data from cantera for T-S diagram
% Tdata = xlsread('T-s.xls',1,'B8:B232');
% Sdata = xlsread('T-s.xls',1,'F8:F232');
% Tdata1=Tdata/T1;
% Sdata1=Sdata/Cp;
```

Friction

Initialize

```
D=0.25;
p1=101325;T1=300; R=573;
v1=R*T1/p1;  %Initial v1
gam=1.4014; M0=0.41223200;
v0=1/5.06812290*v1; p0=32.0637928*101325;
t0=p0*v0/R; T0=t0*(1+(gam-1)/2*M0^2);
P0=p0*(1+(gam-1)/2*M0^2)^(gam/(gam-1));
% Use previous value of alpha
xmin=0; %xmax=12;
dx0=1e-01;
```

Combined flow model:While loop

```
tic
f0=0.000001;
E=10; fmax=0.01;
ff=linspace((f0+fmax)/10,fmax,7);
frc(1:3)=[f0, 100*f0, (f0+fmax)/20];
frc(4:10)=ff;
for e=1:E
    i=1; Mcomp=M0;
    while (Mcomp<0.99)
         if (Mcomp<0.9)
             dx=dx0;
```

```
        elseif (Mcomp<0.95)
            dx=dx0/5;
        else
            dx=dx0/20;
        end
        if (mod(i,10000)==0)
            Mcomp,i
        end
        if (i==1)
           M(i)=M0;
           T(i)=T0;
           p(i)=p0;
           x(i)=xmin;
        else
            Mx=M(i-1);
            Tx=T(i-1);
            px=p(i-1);
            psi=1+(gam-1)/2*Mx^2;
            dTdx=alpha*dx;
            dMdx=Mx*(4*frc(e)/D*gam*Mx^2*psi/2/(1-Mx^2)+.....
dTdx/Tx*(1+gam*Mx^2)*psi/2/(1-Mx^2));
            M(i)=Mx+dx*dMdx;
            T(i)=Tx+dx*dTdx;
            p(i)=px*Mx/M(i)*(T(i)*psi/Tx/(1+(gam-1)/2*M(i)^2))^0.5;
            x(i)=x(i-1)+dx;
        end
```

```
        t(i)=T(i)/(1+(gam-1)/2*M(i)^2);
        P(i)=p(i)*(1+(gam-1)/2*M(i)^2)^(gam/(gam-1));
        v(i)=R*t(i)/p(i);
        Mcomp=M(i);
        dsfr(i)=Cp*log(t(i)/T1)-R*log(p(i)/p1); % addition
        i=i+1;
    end
    str_n(e)=i-1;
    str_t(e,:)=t;
    str_ds(e,:)=dsfr;
    str_p(e,:)=p;
    str_v(e,:)=v;
end
toc
Mcomp =

   0.979756542138573


i =

       10000

Elapsed time is 3.320929 seconds.
```

Plots Pv

```
figure(1)
plot(v2v1,p2p1,'k-','linewidth',2); hold on;
plot(1,1,'k*','linewidth',6);
plot(v3v1,p3p1,'k-.','linewidth',2);
plot([1,vcjv1],[1,pcjp1],'k--','linewidth',2)
plot (0.593,16.71,'kx','linewidth',10) % CJ  point
plot(1/5.06812290,32.0637928,'ko','linewidth',3)
plot([1/5.06812290,1/1.8384],[32.0637928,18.653],'k-','linewidth',3)
plot(v4v1,p4p1,'r-.','linewidth',3);
for e=1:E
   pp=plot(str_v(e,1:str_n(e))/v1,str_p(e,1:str_n(e))/p1);
   if (e~=1)
'LegendInformation'),'IconDisplayStyle','off')
   end
end
hold off;
axis([0.1 max(v2v1) 0 max(p3p1)])
set(gca,'FontSize',15)
set(gca,'FontName','Times')
xlabel('$v_1/v_0$','FontSize',15,'FontName','Times', ...
'Interpreter', 'latex')
ylabel('$P_1/P_0$','FontSize',15,'FontName','Times', ...
'Interpreter', 'latex')
legend('Inert Hugoniot','Initial point', ...
'Heat addition Hugoniot','Rayleigh line',...
```

```
'CJ point','ZND point','ZND to CJ from Cantera', ...
'Rayleigh transition:ZND to CJ'...
,'Combined flow model with friction','Unique Hugoniot')
hold off
```

Plot TS

```
figure(2)
plot(ds12/R,T2T1,'k-','linewidth',2);hold on;%ds14,T4T1,'b:' inert
plot(0,1,'k*','linewidth',6)%initial point
plot(ds13/R,T3T1,'k-.','linewidth',2); % Heat addition
plot(ds1cj/R,TcjT1,'kx','linewidth',10); % CJ point
plot(ds1znd/R,TzndT1,'ko','linewidth',3); % ZND point
plot(ds14/R,T4T1,'b--','linewidth',2)% Transition

for e=1:E
    tt=plot((str_ds(e,1:str_n(e)))/R,str_t(e,1:str_n(e))/T1);
    if (e~=1)
       set(get(get(tt,'Annotation'),'LegendInformation')...
,'IconDisplayStyle','off')
   end
end
plot(ds17/R,T7T1,'b-.','linewidth',2)
plot(ds18/R,T8T1,'b-.','linewidth',2)
hold off;
set(gca,'FontSize',15)
set(gca,'FontName','Times')
```

```
xlabel('$\Delta s/R$','FontSize',15,'FontName','Times', ...
'Interpreter','latex')
ylabel('$T_1/T_0$','FontSize',15,'FontName','Times', ...
'Interpreter','latex')
legend('Inert Hugoniot','Initial point','Heat addition Hugoniot',...
'CJ Point','ZND point','Rayleigh transition',....
    'Combined flow model with friction','Unique Hugoniots')
```

APPENDIX C

CANTERA CODE FOR H_2-O_2 SIMULATION

```
%This program solves for the post-detonation wave variables
%using a ZND model.
%This should then be placed into the RDWE code and iterated.

clear;clc;      %remove when placed in a larger program

%Initial mixture states for the detonation wave
P1 = 101325;
T1 = 300;
q = 'H2:2 O2:1';
mech = 'h2o2_highT.cti';

%Premix speed of sound (change m if not stoichiometric H2-air!)
gas = GRI30;
set(gas, 'Temperature', T1, 'Pressure', P1, 'MoleFractions',  ...
'H2:2,O2:1');
T_1 = temperature(gas);              %Temperature, K
P_1 = pressure(gas);                 %Pressure, Pa
rho_1 = density(gas);                %Density, kg/m^3
S_1 = entropy_mass(gas);             %Entropy, J/(kg K)
X_1 = moleFractions(gas);            %Post-detonation mole fractions
h_1 = enthalpy_mass(gas);            %Enthalpy, J/(kg K)
a_1 = soundspeed(gas);               %Post-detonation SOS, m/s
cp_1 = cp_mass(gas);                 %cp, J/(kg K)
cv_1 = cv_mass(gas);                 %cv, J/(kg K)
m_1 = meanMolecularWeight(gas);      %Molecular weight
```

```
gamma_1 = cp_1/cv_1;              %Specific heat ratio
R_1 = 8314.472/m_1;                %Gas constant, kJ/(kg K)

%Use Cal-Tech SD Toolbox programs to calculate ZND solution
[cj_speed,gas2] = znd_CJ(1, P1, T1, q, mech, 'h2o2', 2);

%Recall properties of the post-ZND gas mixture
T_ZND = temperature(gas2);              %Temperature, K
P_ZND = pressure(gas2);                 %Pressure, Pa
rho_ZND = density(gas2);                %Density, kg/m^3

S_ZND = entropy_mass(gas2);             %Entropy, J/(kg K)
V_ZND = cj_speed;                       %Propagation speed, m/s
X_ZND = moleFractions(gas2);       %Post-detonation mole fractions
h_ZND = enthalpy_mass(gas2);            %Enthalpy, J/(kg K)
a_ZND = soundspeed(gas2);               %Post-detonation SOS, m/s
cp_ZND = cp_mass(gas2);                 %cp, J/(kg K)
cv_ZND = cv_mass(gas2);                 %cv, J/(kg K)
m_ZND = meanMolecularWeight(gas2);      %Molecular weight

%Calculate additional properties after the wave
gamma_ZND = cp_ZND/cv_ZND;              %Specific heat ratio
R_ZND = 8314.472/m_ZND;                 %Gas constant, kJ/(kg K)
M_ZND = V_ZND/a_1;                 %Detonation Mach number
```

REFERENCES

[1] P. A. Thompson, *Compressible Fluid Dynamics*. McGraw-Hill, 1972.

[2] M. D. Salas, "The curious events leading to the theory of shock waves," *Shock waves*, vol. 16, p. 477487, 2007.

[3] K. K. Kuo, *Principles of Combustion*. John Wiley and Sons, 1986, ch. 4.1.

[4] W. Fickett and W. C. Davis, *Detonation Theory and Experiment*. Dover Publications Inc, 2000, ch. 1.

[5] A. H. Shapiro, *The Dynamics and Thermodynamics of Compressible Fluid Flow*. Ronald Press, 1953, vol. 1.

[6] D. L. Chapman, "Rate of explosion in gases," *Philos Mag*, vol. 14, pp. 1091–1094, 1899.

[7] J. Jouguet, "Propagation of chemical reactions in gases," *J.de Mathematiques Pures et Appliquees*, vol. 1, p. 347425, 1905.

[8] Y. B. Zeldovich, "Theory of the propagation of detonation in gaseous systems," *Zhurnal Experimentalnoi i Teoreticheskoi Fizik*, vol. 10, p. 542568, 1940, available in translation as NACA TM-1261.

[9] Y. B. Zeldovich and A. S. Kompaneets, *Theory of Detonation*. Academic Press, NY, 1960, ch. 4.1, english translation of original Russian.

[10] Y. B. Zeldovich and Y. P. Raizer, *Physics of Shock Waves and High-Temperature Hydrodynamic Phenomena*. Wiley, NY, 1966, vol. 1 and 2, ch. 10.

[11] J. von Neumann, *Theory of detonation waves-John von Neumann, Collected Works*. Macmillan, 1942.

[12] W. Doring, "Detonation processes in gases," *Ann. Phys*, vol. 43, p. 421436, 1943, available in translation as NACA TM-1261.

[13] J. Z. S. Browne and J. E. Shepherd, "Numerical solution methods for shock and detonation jump conditions," Aeronautics and Mechanical Engineering California Institute of Technology Pasadena, CA USA 91125, Tech. Rep. FM2006.006 http://www.galcit.caltech.edu/EDL/public/cantera/doc/tex/ShockDetonation/ShockDetonation.pdf.

[14] J. N. Johnson and R. Cheret, "Classic papers in shock compression science," *Springer*, 1998.

[15] A. N. Dremin, *Towards detonation Theory.* Springer, 1999, ch. 2.2.

[16] R. Petela, "Application of exergy analysis to the hydrodynamic theory of detonation in gases," *Fuel Processing Technology*, vol. 67, no. 2, pp. 131 – 145, 2000.

[17] J. Kentfield, "Thermodynamics of airbreathing pulse-detonation engines," *Journal of Propulsion and Power*, vol. 18, no. 6, pp. 1170–1175, 2002.

[18] W. H. Heiser and D. T. Pratt, "Thermodynamic cycle analysis of pulse detonation engines," *Journal of Propulsion and Power*, vol. 18, no. 1, pp. 68–76, 2002.

[19] H. Mirels and J. F. Mullen, "Small perturbation theory for shock-tube attenuation and nonuniformity," *Physics of Fluids*, vol. 7, no. 8, pp. 1208–1218, 1964.

[20] I. Glass and J. P. Sislian, *Nonstationary flows and shock waves.* Oxford University Press, 1994.

[21] F. J. Zeleznik and S. Gordon, "A general i b m 704 or 7090 computer program for computation of chemical equilibrium compositions, rocket performance and chapman-jouguet detonations," NASA, Tech. Rep. Technical Note TN-1454, 1962.

[22] D. G. Goodwin, "Cantera user's guide," Division of Engineering and Applied Science ,California Institute of Technology, Pasadena, CA USA, Tech. Rep., 2001.

[23] M. J.Zucrow and J. D. Hoffman, *Gas dynamics multidimentional Flow.* John Wiley and sons, 1976, vol. 1, ch. 9.

[24] B. Hodge and K. Koenig, *Compressible Fluid Dynamics with Personal Computer Applications.* Prentice-Hall, 1995.

BIOGRAPHICAL STATEMENT

Sushma Rao was born in Bangalore, India on January 15, 1982, to Sudha and Sudheendra Rao. She was raised in the cosmopolitan suburb of Vashi, Navi Mumbai. Sushma received a B.Arch. degree in Architecture from the University of Mumbai, in 2004. During her career as an Architect, Sushma was involved in designing multi-storied buildings as well as interiors for corporate offices. After working for three and a half years as an Architect, she joined the University of Texas at Arlington (UTA) for a Masters in Aerospace Engineering.

At UTA, Sushma's interests were mainly in fluids and controls, although she also enjoyed the odd course in Automobile Engineering. She decided to work in the area of pulse detonation engines for her thesis with Prof. Frank Lu. During the last semester of her Masters, Sushma worked as an intern at the Center for Space Nuclear Research at Idaho National Laboratories, Idaho, USA. Her work involved feasibility studies of a sample return mission from Mars.

During her graduate studies, Sushma married her long time boyfriend Pratik Donde.

Sushma's interest outside academia include hiking and other adventure sports. She has trekked various peaks in the Himalayas and Western Ghats in India, and also in the Rocky Mountains of Idaho, USA.